Upper-Tropospheric Low Richardson Number in Tropical Cyclones: Sensitivity to Cyclone Intensity and the Diurnal Cycle

PATRICK DURAN AND JOHN MOLINARI

Department of Atmospheric and Environmental Sciences, University at Albany, State University of New York, Albany, New York

(Manuscript received 24 April 2015, in final form 7 October 2015)

ABSTRACT

High-vertical-resolution rawinsondes were used to document the existence of low–bulk Richardson number (R_b) layers in tropical cyclones. The largest frequency of low R_b existed in the inner 200 km at the 13.5-km level. This peak extended more than 1000 km from the storm center and sloped downward with radius. The presence of an extensive upper-tropospheric low-R_b layer supports the assumption of Richardson number criticality in tropical cyclone outflow by Emanuel and Rotunno.

The low-R_b layers were found to be more common in hurricanes than in tropical depressions and tropical storms. This sensitivity to intensity was attributed to a reduction of upper-tropospheric static stability as tropical cyclones intensify. The causes of this destabilization include upper-level cooling that is related to an elevation of the tropopause in hurricanes and greater longwave radiative warming in the well-developed hurricane cirrus canopy. Decreased mean static stability makes the production of low R_b by gravity waves and other perturbations easier to attain.

The mean static stability and vertical wind shear do not exhibit diurnal variability. There is some indication, however, that low Richardson numbers are more common in the early morning than in the early evening, especially near the 200–300-km radius. The location and timing of this diurnal variability is consistent with previous studies that found a diurnal cycle of infrared brightness temperature and rainfall in tropical cyclones.

1. Introduction

Turbulence associated with tropical cyclones (TCs) can considerably disrupt aviation traffic. Although severe turbulence is most often observed within 100 km of active convection (Lane et al. 2012), widespread turbulence also has been reported in the upper-level outflow of mesoscale convective systems several hundred kilometers away from convection (Trier and Sharman 2009). Possible causes of this turbulence include breaking gravity waves (Lane et al. 2012) and strong vertical wind shear associated with MCS outflow (Zovko-Rajak and Lane 2014). Although turbulence near midlatitude MCSs has been studied extensively, little work has been done to address turbulence near TCs.

In their theoretical framework, Emanuel and Rotunno (2011) proposed that the hurricane outflow layer develops its own temperature stratification by a requirement that small-scale turbulence maintains the Richardson number near a critical value. This closure directly coupled low Richardson number to vortex structure and intensification (Emanuel 2012). This suggests a fundamental role for outflow-layer turbulence and a need to examine turbulence in observations.

Using three-dimensional simulations of Hurricane Rita (2005), Fovell and Su (2007) found that changing the microphysics parameterization produced large variations in storm motion that led to track-forecast spread comparable to that of a multimodel ensemble. Subsequent work (Fovell et al. 2009, 2010) showed that TC track, structure, and intensity all are sensitive to microphysical assumptions. This sensitivity is related to the interaction of cloud particles with radiation (cloud–radiative feedback), which modifies the radial pressure gradient as a result of within-cloud warming. These results were corroborated by Bu et al. (2014),

Corresponding author address: Patrick Duran, Department of Atmospheric and Environmental Sciences, University at Albany, State University of New York, ES 351, 1400 Washington Ave., Albany, NY 12222.
E-mail: pduran@albany.edu

DOI: 10.1175/JAS-D-15-0118.1

who found that the net effect of cloud–radiative feedback is to broaden the primary circulation and strengthen the secondary circulation. The vertical structure of radiative forcing in their simulations (cf. their Fig. 7c) exhibits weak warming between 7 and 12 km and strong cooling immediately above, which indicates a potential destabilization of the outflow layer by radiative effects. A limitation of their approach, however, is that they averaged their results over the diurnal radiative cycle and thus did not address diurnal variability.

It is well known that TCs exhibit a diurnal cycle (e.g., Kossin 2002), but the mechanisms that drive it have not been fully elucidated. Dunion et al. (2014) provided unprecedented documentation of this cycle using 6-hourly infrared brightness temperature differences. They found that a burst of low infrared brightness temperatures arises near the TC center overnight. These low brightness temperatures then propagate radially outward at a speed of about 5–10 m s^{-1}, taking on the form of a ring as cloud tops warm radially inward of the lowest brightness temperatures. The ring reaches the 200–300-km radius around 0800 local standard time (LST), and the 300–400-km radius by around local noon. The timing of this ''diurnal pulse'' feature was found to be consistent between storms and across oceanic basins. They proposed five mechanisms that may contribute to the diurnal cycle, four of which invoke changes in the horizontal or vertical structure of radiative heating within the cirrus canopy throughout the day. They also presented some limited evidence that the upper-level cirrus pulse is coupled to convection. This argument was corroborated in part by Bowman and Fowler (2015), who found a diurnal cycle in TC rainfall rate with a maximum at 0600 LST and a minimum at 1800 LT. It is possible that the upper-tropospheric Richardson number has a diurnal cycle consistent with the observed diurnal cycles of cirrus and rainfall.

Molinari et al. (2014) examined bulk Richardson number R_b in TCs using NOAA Gulfstream-IV (G-IV) dropsondes. They found a steady increase in the frequency of low–Richardson number layers above the 9-km level to a peak near 13 km. These layers most often coexisted with low static stability in the upper troposphere, consistent with the in-cloud heating and cloud-top cooling given by Bu et al. (2014). Because the G-IV dropsonde data rarely extend above the 13-km height, they could not measure the full cirrus canopy, which can reach 16 km (Waco 1970). The rawinsondes used in the present study provide high-resolution data well into the stratosphere. In addition, they sample twice daily and observe a wider range of storm intensity than the G-IV dropsondes. The rawinsonde data will allow the following questions to be addressed:

- What is the radial–vertical structure of the Richardson number above 13 km?
- How does upper-tropospheric Richardson number vary with storm intensity?
- How does upper-tropospheric Richardson number change with time of day?

2. Data and methods

The U.S. High Vertical Resolution Radiosonde Data archive (Love and Geller 2012) is used to construct the radial–vertical structure of TC outflow. All sondes released within 1000 km of Atlantic basin TCs from 1998 to 2011 are used, including special soundings released at 0600 and 1800 UTC. The dataset includes sondes released from the eastern United States, the Bahamas, Puerto Rico, Grand Cayman, and Belize. Herein we analyze the vertical layer between 9 and 17 km, which is at the upper limit of—or above—the analyses performed by Molinari et al. (2014).

Storm center positions are determined using the National Hurricane Center Atlantic basin hurricane database (HURDAT; Jarvinen et al. 1984). For the 1998–2011 time interval, HURDAT contained 1807 hurricane, 2500 tropical storm, and 1192 tropical depression analysis times. Sondes are separated into 200-km radial bins about a composite TC center, with each bin overlapping the adjacent bins by 100 km. This binning ensures that there are sufficient observations in each bin for azimuthal averaging but does not allow for the TC inner core to be resolved.

Every sounding was visually examined to ensure quality, and 218 questionable soundings—constituting less than 3% of the total number—were removed. Of these 218 soundings, 130 were removed because data gaps larger than 1 km arose in the 9–17-km layer; another 84 were removed because they contained upper-tropospheric vertical wind shears larger than 40 m s^{-1} km^{-1}; and 3 were removed because they contained multiple observations on the same pressure level.

As in Molinari et al. (2014), the remaining 8499 soundings were interpolated to 100-m vertical levels and smoothed using a 1–2–1 smoother. The bulk Richardson number

$$R_b = \frac{(g/\theta_v)(\Delta\theta_v/\Delta z)}{[(\Delta u)^2 + (\Delta v)^2]/(\Delta z)^2}, \quad (1)$$

where $\overline{\theta_v}$ is the layer-averaged virtual potential temperature, was then computed for 400-m (Δz) layers

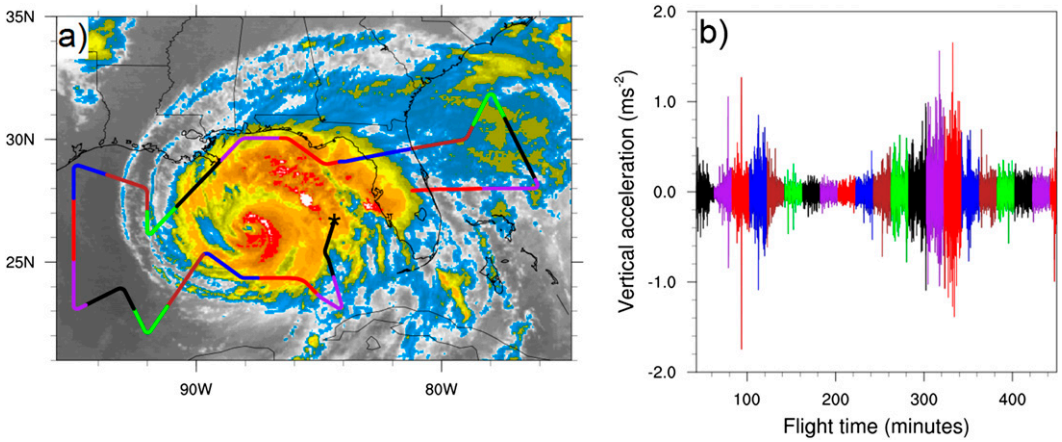

FIG. 1. (a) The G-IV flight track into Hurricane Ivan between 0530 and 1310 UTC 15 Sep 2005 overlaid on an infrared satellite image valid at 0915 UTC. (b) Time series of aircraft vertical acceleration observed by the G-IV inertial navigation system. The initial time for both plots is indicated by the black asterisk in (a), and the color changes in the flight track correspond to the color changes in (b). All data plotted here were collected while the G-IV was at an altitude of 12 km or greater.

centered on each level. The percentage of rawinsondes that observe $R_b < 0.25$ is plotted as a composite radius–height cross section, along with the azimuthally averaged stability and shear contributions to R_b [azimuthal averages of the numerator and denominator of Eq. (1), respectively]. These components of R_b are plotted as difference fields to show variability with TC intensity and time of day, and the statistical significance of these differences is tested using a 10 000 sample bootstrapping technique. Probability distributions also are used to assess the contribution of transient perturbations to the generation of low-R_b layers. To avoid double counting, these probability distributions do not use overlapping bins.

To aid in the diagnosis of changes in upper-tropospheric structure, average tropopause heights are calculated for each intensity and time stratification. The tropopause height is determined for each sounding using the following World Meteorological Organization definition: "the lowest level at which the lapse rate decreases to 2°C km^{-1} or less, provided that the average lapse rate between this level and all higher levels within 2 km does not exceed 2°C km^{-1} (WMO 1957). The tropopause heights are then averaged using the same radial binning as the R_b fields and overlaid on the stability and shear cross sections.

Flight-level vertical accelerations observed by the G-IV aircraft, recorded at a frequency of 1 Hz in Hurricane Ivan (2004), are used to provide an example of upper-tropospheric turbulence. All observations used herein were recorded while the aircraft was above the 12-km altitude. The G-IV's true airspeed for these data varies between 220 and 242 m s^{-1}, placing the horizontal spacing of observations at around 230 m.

3. Results

a. *Aircraft turbulence observations*

Given that aircraft often observe turbulence while flying in the outflow of mesoscale convective systems, we first consider turbulence observed on an aircraft in the vicinity of a hurricane. Vertical acceleration from a G-IV flight into Hurricane Ivan (2004) is shown in Fig. 1, along with the flight track overlaid on an infrared satellite image. Plotting begins at the black asterisk, and changes in the color of the flight track corresponding to changes in the color of the vertical acceleration trace.

The area within the cirrus canopy is more turbulent than the clear air surrounding the storm (Fig. 1). As the aircraft enters the cirrus region, the vertical acceleration exhibits considerably larger variance, and the variance remains elevated until the aircraft exits the cirrus canopy. As the G-IV turns eastward and repenetrates the cirrus, the vertical acceleration variance again increases and remains elevated until the aircraft once again exits the storm. The observations here are not collected in the inner core of strong convection, but in high-cloud regions at outer radii. Thus, the turbulence is not likely to be the direct result of strong mesoscale convection, but instead the consequence of other mechanisms unique to the cirrus canopy and the near-storm environment. Although the magnitude of the accelerations corresponds to only light turbulence (WMO 1998), such a striking difference between the within-cirrus and clear-air

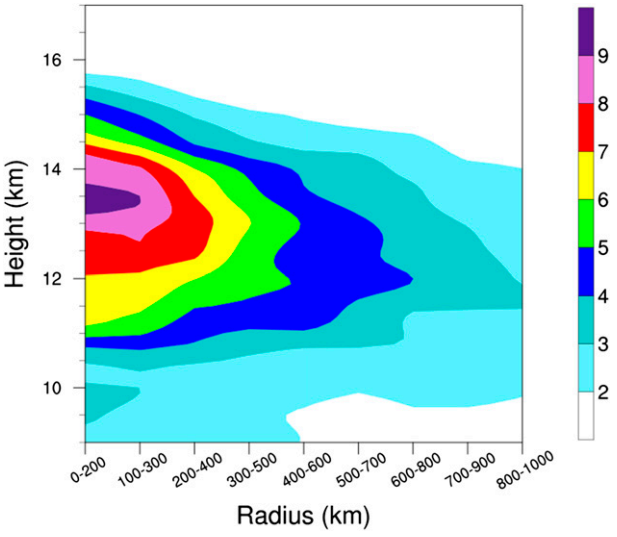

FIG. 2. Radius–height cross section of the percentage of rawinsondes that observe a bulk Richardson number less than 0.25 for all available sondes released within 1000 km of an Atlantic basin tropical cyclone. Because vertical resolution is much larger than radial resolution, a 1–2–1 smoother is applied in the vertical 10 times for plotting purposes.

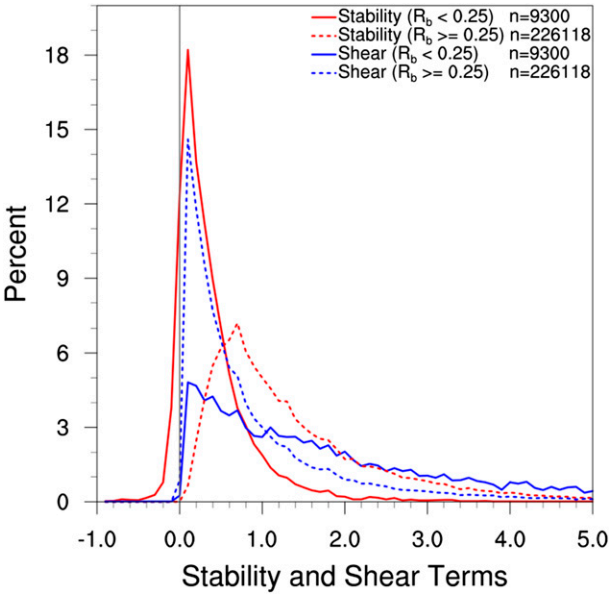

FIG. 3. Probability distributions of the static stability and vertical wind shear terms (10^{-4} s^{-2}) of the bulk Richardson number for all data points between the 11- and 15-km levels. Red curves represent static stability and blue curves represent vertical wind shear. Solid curves are for all points where the bulk Richardson number is smaller than 0.25, and dotted curves are for points where the bulk Richardson number is greater than or equal to 0.25. The small number of apparently negative shear-squared values is an artifact of the use of finite bins in the plotting routine.

environments suggests that there exist mechanisms unique to the cirrus canopy that produce turbulence.

b. *Low Richardson number, stability, and shear in the upper troposphere*

The occurrence of low R_b in the upper troposphere of TCs is illustrated in Fig. 2, using all soundings in the dataset. The frequency of $R_b < 0.25$ decreases outward from a maximum of over 9% at inner radii to 2%–3% at 1000 km. At inner radii, low-R_b frequency is maximized near the 13.5-km level, whereas at outer radii the maximum is near 11.5 km. A downward radial slope is present throughout the composite along with a gradual thinning of the low-R_b layer with increasing radius.

The static stability and vertical wind shear terms of R_b [the numerator and denominator of Eq. (1), respectively] for all data points between the 11- and 15-km levels are shown in Fig. 3. The distributions of static stability (red lines) and vertical wind shear (blue lines) both are maximized near zero and fall off rapidly with increasing values. The lack of a left tail in the distributions is a consequence of the physical nature of the static stability and vertical wind shear terms: in the absence of strong forcing, a static stability less than zero should be rapidly mixed out, so negative static stabilities are rare, and the vertical wind shear term is defined to be greater than zero.

The static stability distribution for points with $R_b <$ 0.25 (solid red line) is shifted toward smaller values relative to the same distribution for data points that observe larger R_b (dotted red line). This indicates that local decreases in static stability contribute to the generation of low-R_b layers. Similarly, the vertical wind shear distribution for all data points with $R_b < 0.25$ (solid blue line) is shifted toward larger values relative to the same distribution for data points that observe larger R_b (dotted blue line). The upper tail of this distribution extends to very large values, indicating that high-magnitude vertical wind shear perturbations also contribute to the generation of low-R_b layers.

These results are consistent with Molinari et al. (2014), who found that the frequency of low R_b is maximized in the upper troposphere, and that both static stability and vertical wind shear perturbations contribute to its production.

c. *Variation of Richardson number with TC intensity*

Stratifying the soundings by intensity reveals striking differences in the upper-tropospheric environments of hurricanes and weak TCs (tropical depressions and tropical storms). Hurricanes (Fig. 4a) exhibit a broad region where more than 21% of sondes observe $R_b <$ 0.25 at any given level, extending past the 100–300-km

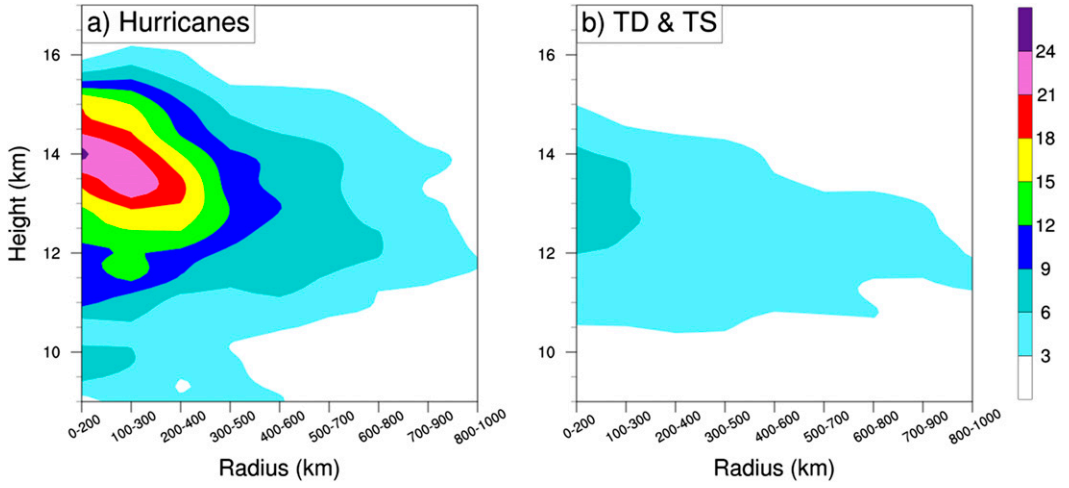

FIG. 4. As in Fig. 2, but for all sondes released within 1000 km of (a) hurricanes and (b) tropical depressions and tropical storms.

radial bin (note that the scale differs from that in Fig. 2). Weak TCs (Fig. 4b), on the other hand, possess a more radially confined maximum of less than 9%.

In hurricanes, the maximum frequency of $R_b < 0.25$ at the inner radii is centered near 14-km altitude, whereas in weak TCs it occurs near 13 km. The largest frequency of $R_b < 0.25$ in hurricanes—indicated by the warm colors—exhibits a much steeper downward radial slope at the inner radii than that observed in all storms (Fig. 2). At all radii, low R_b extends to higher altitudes in hurricanes than in weak TCs, and larger frequencies of $R_b < 0.25$ extend much farther radially outward.

The differences between the azimuthally averaged numerator and denominator of Eq. (1) for hurricanes and weak TCs are plotted in Figs. 5a and 5b, respectively. These differences represent hurricane values minus those for weak TCs, such that regions shaded in red exhibit larger values in hurricanes, and regions shaded in blue exhibit smaller values. Solid orange lines represent the tropopause height for hurricanes and dashed lines are for weak TCs.

Static stability within the upper troposphere of hurricanes is considerably smaller than that in weak TCs (Fig. 5a), a pattern that extends past the 1000-km radius. The stability differences encompassed by the blue shading are associated with lapse rate differences ranging from approximately 0.5 (lightest blue) to 2 K km^{-1} (darkest blue). Thus, the lapse rate difference between the two intensity classes is a significant fraction of the dry adiabatic lapse rate throughout much of the upper troposphere. This difference is significant at the 99% confidence interval for most data points in the 12–16-km layer.

Two layers of enhanced vertical wind shear exist in hurricanes: one centered near 16-km altitude and another near 11.5 km (Fig. 5b). The upper layer of enhanced shear is strong, with some differences exceeding 10 m s^{-1} km^{-1} (shear-squared term of 10^{-4} s^{-2}). Within an extensive portion of this enhanced shear layer, however, the static stability is too large to allow R_b to fall below 0.25. The lower-altitude enhanced shear layer exhibits maximum differences between 6.3 and 7.7 m s^{-1} km^{-1} (shear-squared term of 0.4 and 0.6 $\times$ 10^{-4} s^{-2}, respectively). This layer lies within a region of smaller static stability than the upper shear layer and appears to be associated with some increased frequency of $R_b < 0.25$ at the inner radii in hurricanes (Fig. 6). On the other hand, large R_b differences exist even in regions where the mean vertical wind shear differences are zero. For example, at 14-km altitude in the 0–200-km radial bin—where the frequency of $R_b < 0.25$ is maximized in hurricanes—the difference in low R_b frequency between hurricanes (Fig. 4a) and weak TCs (Fig. 4b) is approximately 18%. This same region, however, is characterized by slightly smaller vertical wind shear in hurricanes than in weak TCs (Fig. 5b). Thus, although increased mean vertical wind shear can contribute to increased frequencies of low R_b, it does not appear to be a necessary ingredient.

Decreasing mean static stability is accomplished through a combination of average warming below 14 km and average cooling above as TCs intensify (Fig. 6). Hurricanes are at least 1 K warmer than weak TCs throughout most of the mid- to upper troposphere, with a maximum warm anomaly of greater than 3 K at the inner radii. Above about 15 km, hurricanes are cooler than weak TCs, with a maximum cold anomaly of

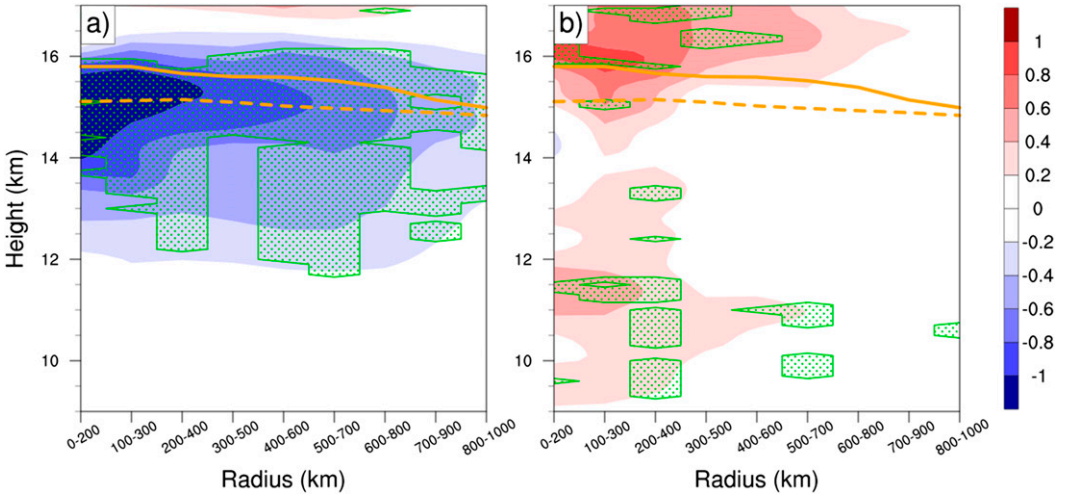

FIG. 5. Radius–height cross sections of the differences in azimuthally averaged (a) numerator (stability) and (b) denominator (shear) of Eq. (1) in hurricanes vs weak TCs. The difference (10^{-4} s^{-2}) is plotted such that blue colors represent values that are smaller in hurricanes than in weak TCs. Because vertical resolution is much larger than radial resolution, a 1–2–1 smoother is applied in the vertical 10 times for plotting purposes. The solid orange line is the average tropopause height for hurricanes, and the dashed orange line is the average for weak TCs. Green stippling indicates regions where the differences are statistically significant at the 99% confidence interval.

greater than 4 K extending past the 200–400-km radial bin.

These temperature differences can arise due to a combination of a number of processes. As a TC intensifies, boundary layer equivalent potential temperature θ_e increases near the vortex center. Accordingly, the buoyancy of rising air parcels increases, allowing them to penetrate into the lower stratosphere. Since the moist lapse rate approaches dry adiabatic in the upper levels, strong adiabatic cooling can occur for moist ascent in the upper troposphere and lower stratosphere. This strong cooling partially manifests as an elevation of the average tropopause and a destabilization of the layer above 15 km, as seen in Fig. 5a. This is consistent with the findings of Jordan and Jordan (1954) and Koteswaram (1967), who observed an elevated tropopause and a layer of near-neutral static stability in the upper troposphere, especially at the inner radii.

As a TC vortex intensifies, the magnitude of its mid- to upper-tropospheric warm anomaly increases, consistent with balanced dynamics. This strengthening warm core is clearly present below 14 km at the inner radii in Fig. 6. In addition, both observational (Garrett et al. 2005) and modeling (Bu et al. 2014) studies indicate that radiative cooling dominates the top layer of thick anvil cirrus. In their idealized simulations of an intense hurricane, Bu et al. (2014) found that, averaged over the diurnal cycle, the 12–16-km layer is characterized by net radiative cooling extending past the 300-km radius. Immediately below this cooling layer exists a broad region of weak radiative warming that reaches a maximum near 11-km altitude. The temperature difference structure in Fig. 6 is consistent with these modeling results. Thus, it is plausible that radiative tendencies combine with adiabatic cooling near the tropopause to produce the lower-stability layer in hurricanes seen in Fig. 5a. Regardless of

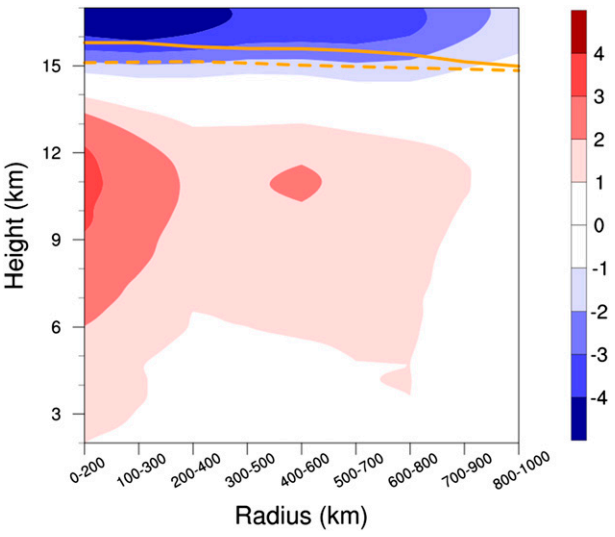

FIG. 6. Radius–height cross section of the azimuthally averaged temperature (K) in hurricanes minus that in tropical depressions and tropical storms, such that blue colors represent lower temperatures in hurricanes. Because vertical resolution is much larger than radial resolution, a 1–2–1 smoother is applied in the vertical 10 times for plotting purposes. The solid orange line is the average tropopause height for hurricanes, and the dashed orange line is the average tropopause height for weak TCs.

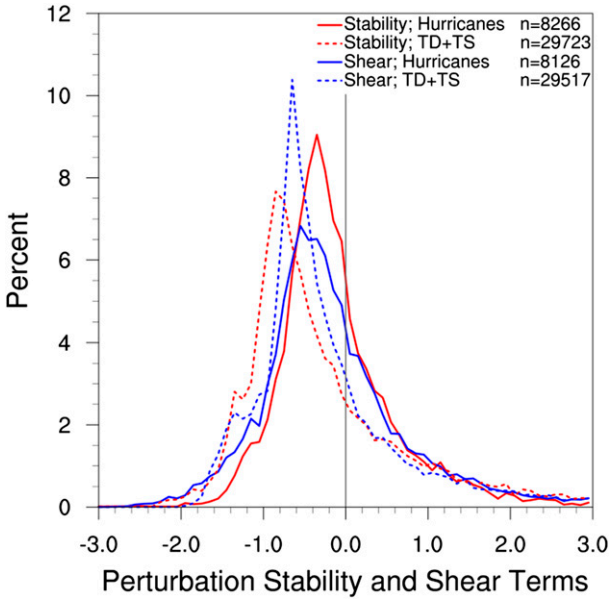

FIG. 7. Probability distributions of the perturbation static stability and vertical wind shear terms ($10^{-4}\,s^{-2}$) of the bulk Richardson number for hurricanes and weak TCs. Perturbations are computed by subtracting the azimuthal average from each individual observation within the 400-km radius and between the 11- and 15-km levels, using 100-km-wide, nonoverlapping radial bins. The physical characteristics of static stability and vertical wind shear cause the perturbation distributions to be primarily negative, as discussed in section 3c.

the mechanisms, the presence of this low-stability layer means that only small perturbations are required to decrease the bulk Richardson number to a value below 0.25.

Distributions of the perturbation static stability and vertical wind shear are shown in Fig. 7. These perturbations are computed by subtracting the azimuthally averaged static stability and vertical wind shear from each individual observation in the 11–15-km layer and within the 400-km radius. The azimuthal averages here use 100-km nonoverlapping radial bins instead of 200-km overlapping bins to avoid double counting observations in the distributions. Because of the skewness of the static stability and vertical wind shear distributions (see Fig. 3), the azimuthal averages are larger than most of the individual observations in the dataset. As a result, the peaks of the distributions in Fig. 7 are negative.

The perturbation distributions alone are not able to explain why low R_b is more common in hurricanes. The static stability distribution for weak TCs (dotted red line) is shifted toward lower values relative to that for hurricanes (solid red line), indicating that stronger local decreases in static stability occur in weak TCs. This result alone suggests that weak TCs should have a higher frequency of low R_b than hurricanes, but this is not observed. This indicates that the mean static stability is a more important contributor to decreasing R_b in hurricanes than the perturbation static stability. The vertical wind shear distribution is shifted toward higher values in hurricanes (solid blue line) relative to weak TCs (dotted blue line). This indicates that the shear perturbations in hurricanes are more positive (more favorable for low R_b) than in weak TCs. These larger perturbations coexist with larger mean vertical wind shear (Fig. 5b).

The synthesis of these results suggests that the higher frequency of $R_b < 0.25$ in hurricanes is due to a combination of decreased upper-tropospheric mean static stability and increased mean and perturbation vertical wind shear. The perturbation static stability does not appear to contribute to the increased frequency of low R_b in hurricanes.

d. Variation of Richardson number with time of day

To assess whether the TC diurnal cycle described by Dunion et al. (2014) is associated with variations in Richardson number, the upper-tropospheric environment is analyzed for all soundings collected at 0000 and 1200 UTC. Sondes released at 0600 and 1800 UTC are not considered here because their numbers are much fewer and the observations are skewed toward more intense TCs. The exclusion of these sondes from more intense TCs yields a smaller overall frequency of $R_b < 0.25$ in Fig. 8 than in Fig. 4.

Since all sondes were released in the Caribbean and the eastern United States, the 0000 and 1200 UTC composites are representative of the hours near sunset and sunrise, respectively. Considering these opposite extremes of the diurnal cycle—one after extended sunlight and the other after extended darkness—allows for an interpretation of how R_b changes with time of day.

The difference between the frequency of $R_b < 0.25$ observed in the evening (Fig. 8a) and in the morning (Fig. 8b) is considerably smaller than the difference between the two intensity classifications shown in Figs. 4a and 4b. Evidence exists, however, that low R_b is more common in the morning than in the evening. The region in which low R_b is most common at 1200 UTC—near 200 km—is the radius at which the diurnal pulse of cold cloud is expected to be located at 0800 LST. Since the majority of these sondes were released in the eastern time zone, where 1200 UTC corresponds to 0700 LST, these results indicate that the morning maximum of low R_b is located near the radius of the diurnal pulse as described by Dunion et al. (2014).

The diurnal variation of azimuthally averaged static stability (Fig. 9a) and vertical wind shear (Fig. 9b) is small. Upper-tropospheric wind shear

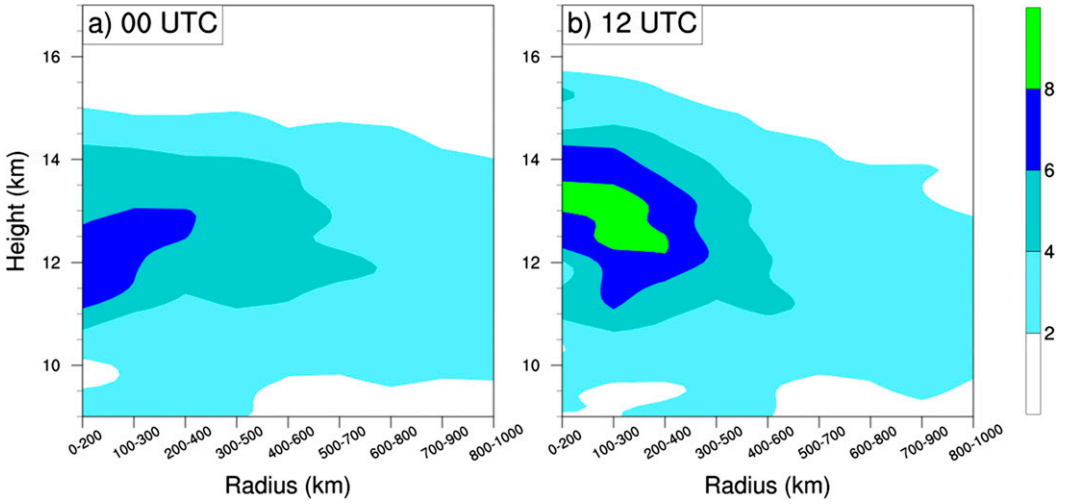

FIG. 8. As in Fig. 4, but for all sondes released at (a) 0000 UTC (evening) and (b) 1200 UTC (morning). Sondes released at 0600 and 1800 UTC are not considered here because their numbers are much fewer and the observations are skewed toward more intense TCs. The exclusion of these sondes from more intense TCs yields a smaller overall frequency of $R_b < 0.25$ here than in Fig. 5.

might be slightly larger in the morning than in the evening, but this difference is not statistically significant. The static stability profile and the tropopause level are nearly identical at 0000 and 1200 UTC. Thus, unlike the intensity variability seen in the previous section, the R_b differences do not appear to be attributable to a more favorable average background state.

Distributions of the perturbation static stability and vertical wind shear (Fig. 10) are shifted toward smaller values in the morning relative to the evening. This indicates that local static stability perturbations are more conducive to low R_b in the morning, while local shear perturbations are less conducive. These results, combined with the lack of a significant difference in the mean fields, suggest that local static stability perturbations may be the driver behind the larger frequency of $R_b < 0.25$ in the morning.

4. Summary and conclusions

High-vertical-resolution rawinsondes were used to document the existence of low–bulk Richardson number layers in tropical cyclones. The peak in $R_b < 0.25$ existed in the inner 200 km at the 13.5-km level. This is

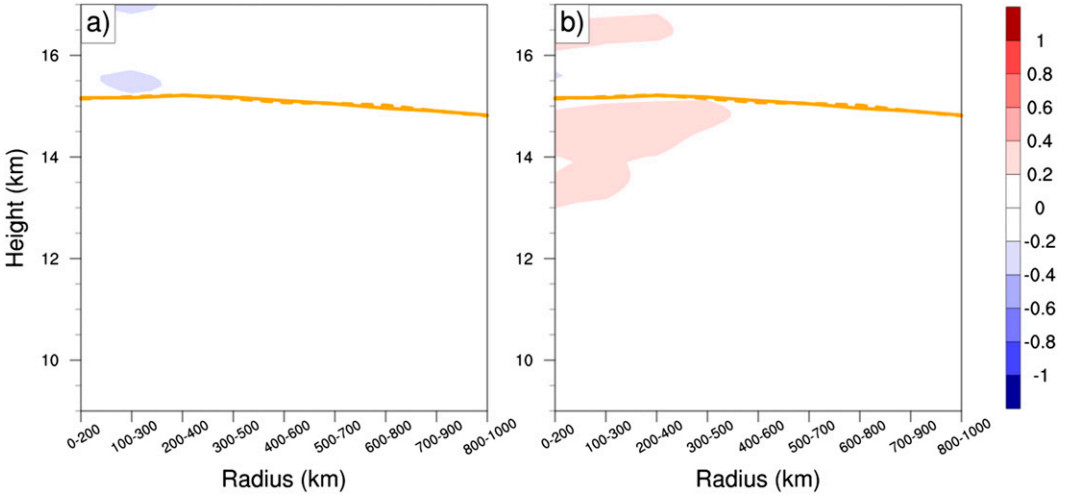

FIG. 9. As in Fig. 5, but for all sondes released at 1200 UTC (morning) minus all sondes released at 0000 UTC (evening), such that blue colors represent values that are smaller at 1200 UTC than at 0000 UTC. The absence of green stippling indicates that these differences are not statistically significant at the 99% confidence interval.

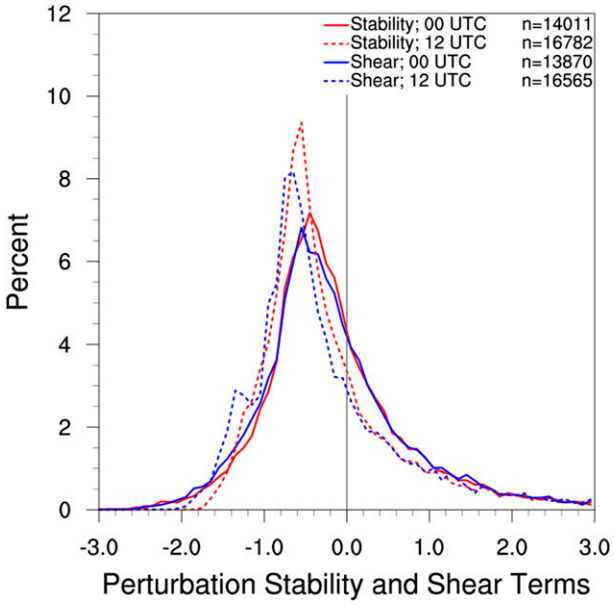

FIG. 10. As in Fig. 7, but at 0000 UTC (solid lines) and 1200 UTC (dotted lines).

consistent with the results of Molinari et al. (2014), but the rawinsondes used here sampled a deeper layer, which allowed for an examination of the tropopause height. The low-R_b maximum extended out past the 1000-km radius, with a steady decrease in the height of the maximum to the 11.5-km level at the outer edge. The presence of an extended upper-tropospheric low–Richardson number layer supports the assumption of Richardson number criticality in tropical cyclone outflow by Emanuel and Rotunno (2011).

The frequency of upper-tropospheric $R_b < 0.25$ was found to be more than twice as large in hurricanes as in weak TCs. The key factor was lower mean static stability in the upper troposphere of hurricanes, which was associated with a warmer midtroposphere and colder upper troposphere. Higher temperatures below 14 km arose from the midtropospheric warm anomaly that is required to maintain thermal wind balance in an intensifying TC. In addition, it is likely that larger radiative heating exists in the hurricane's well-developed and long-lasting cirrus canopy. The upper-tropospheric cooling was accompanied by a 1-km increase in tropopause height in hurricanes, which was associated with much lower static stability in the upper troposphere. It is hypothesized that persistent convection, gravity wave critical-layer interactions, and enhanced radiative cooling near the top of the hurricane cirrus canopy contributed to the development of this cool layer.

The mean fields do not account for local variations in static stability and vertical wind shear that are often responsible for low–Richardson number layers in mesoscale convective systems (Lenz et al. 2009; Trier et al. 2010). The widely spaced rawinsondes employed in this study cannot evaluate the role of such local variations. Instead, the distributions of perturbation stability and shear were compared for hurricanes and weak TCs. Somewhat surprisingly, weaker storms had more frequent negative stability perturbations, but also more frequent positive shear perturbations, with offsetting impacts on Richardson number. The results suggest that the mean field variations might be the predominant factor in the more frequent occurrence of a low Richardson number in hurricanes than in weaker TCs. This more favorable background state makes it more likely that forcing associated with convection, radiative effects, and gravity waves could produce a low Richardson number.

The diurnal variation of the Richardson number was also examined. The mean static stability in the evening was nearly the same as the mean static stability in the early morning. This is surprising given the results of Melhauser and Zhang (2014), which showed that during a perpetual-night simulation, strong radiative cooling at cloud top overlies a layer of longwave warming within cloud. Such a radiative heating profile should act to decrease the upper-tropospheric static stability overnight, but this was not observed in the mean fields. If the TC diurnal cycle is convective in nature, as suggested by Dunion et al. (2014), and supported by Bowman and Fowler (2015), it is possible that by early morning the convection has acted to remove the instability created by these radiative effects. The diurnal variations in Richardson number and perturbation static stability, although small, are at least consistent with the presence of more active convection in the morning.

Recent dropsonde observations from the NASA Global Hawk and WB-57 aircraft show promise in further illuminating how TCs modify their upper-tropospheric environment. Dropsondes are deployed from these aircraft in the stratosphere, allowing an analysis of the full depth of the cirrus canopy. Unlike the rawinsonde composites used here, analyses from these soundings have large spatiotemporal resolution, which allows for a snapshot of the upper troposphere of a single storm. Preliminary work with these data show that very large horizontal temperature variations can arise across the cirrus canopy, and large fluctuations can occur at one location over time. The causes and implications of these large variations are the subject of future work.

Acknowledgments. We thank David Vollaro for assistance with rawinsonde data processing and Charles

Helms and Jason Dunion for insightful discussions of this work. We also thank two anonymous reviewers for their helpful comments on the manuscript. Flight-level datasets were provided by the NOAA/Hurricane Research Division of AOML and rawinsonde observations were obtained from the SPARC Data Center at the Stony Brook University. This research was supported by Office of Naval Research Grant N000141410162 and NASA Grant NNX12AJ81G under the Hurricane Science Research Program.

REFERENCES

Bowman, K. P., and M. D. Fowler, 2015: The diurnal cycle of precipitation in tropical cyclones. *J. Climate*, **28**, 5325–5334, doi:10.1175/JCLI-D-14-00804.1.

Bu, Y. P., R. G. Fovell, and K. L. Corbosiero, 2014: Influence of cloud–radiative forcing on tropical cyclone structure. *J. Atmos. Sci.*, **71**, 1644–1662, doi:10.1175/JAS-D-13-0265.1.

Dunion, J. P., C. D. Thorncroft, and C. S. Velden, 2014: The tropical cyclone diurnal cycle of mature hurricanes. *Mon. Wea. Rev.*, **142**, 3900–3919, doi:10.1175/MWR-D-13-00191.1.

Emanuel, K., 2012: Self-stratification of tropical cyclone outflow. Part II: Implications for storm intensification. *J. Atmos. Sci.*, **69**, 988–996, doi:10.1175/JAS-D-11-0177.1.

——, and R. Rotunno, 2011: Self-stratification of tropical cyclone outflow. Part I: Implications for storm structure. *J. Atmos. Sci.*, **68**, 2236–2249, doi:10.1175/JAS-D-10-05024.1.

Fovell, R. G., and H. Su, 2007: Impact of cloud microphysics on hurricane track forecasts. *Geophys. Res. Lett.*, **34**, L24810, doi:10.1029/2007GL031723.

——, K. L. Corbosiero, and H.-C. Kuo, 2009: Cloud microphysics impact on hurricane track as revealed in idealized experiments. *J. Atmos. Sci.*, **66**, 1764–1778, doi:10.1175/2008JAS2874.1.

——, ——, A. Seifert, and K.-N. Liou, 2010: Impact of cloud-radiative processes on hurricane track. *Geophys. Res. Lett.*, **37**, L07808, doi:10.1029/2010GL042691.

Garrett, T. J., and Coauthors, 2005: Evolution of a Florida cirrus anvil. *J. Atmos. Sci.*, **62**, 2352–2372, doi:10.1175/JAS3495.1.

Jarvinen, B. R., C. J. Neumann, and M. A. S. Davis, 1984: A tropical cyclone data tape for the North Atlantic Basin, 1886–1983: Contents, limitations, and uses. NOAA Tech. Memo. NWS NHC 22, 21 pp. [Available online at http://www.nhc.noaa.gov/pdf/NWS-NHC-1988-22.pdf.]

Jordan, C. L., and E. S. Jordan, 1954: On the mean thermal structure of tropical cyclones. *J. Meteor.*, **11**, 440–448, doi:10.1175/1520-0469(1954)011<0440:OTMTSO>2.0.CO;2.

Kossin, J. P., 2002: Daily hurricane variability inferred from GOES infrared imagery. *Mon. Wea. Rev.*, **130**, 2260–2270, doi:10.1175/1520-0493(2002)130<2260:DHVIFG>2.0.CO;2.

Koteswaram, P., 1967: On the structure of hurricanes in the upper troposphere and lower stratosphere. *Mon. Wea. Rev.*, **95**, 541–564, doi:10.1175/1520-0493(1967)095<0541:OTSOHI>2.3.CO;2.

Lane, T. P., R. D. Sharman, S. B. Trier, R. G. Fovell, and J. K. Williams, 2012: Recent advances in the understanding of near-cloud turbulence. *Bull. Amer. Meteor. Soc.*, **93**, 499–516, doi:10.1175/BAMS-D-11-00062.1.

Lenz, A., K. M. Bedka, W. F. Feltz, and S. A. Ackerman, 2009: Convectively induced transverse band signatures in satellite imagery. *Wea. Forecasting*, **24**, 1362–1373, doi:10.1175/2009WAF2222285.1.

Love, P. T., and M. A. Geller, 2012: Research using high (and higher) resolution radiosonde data. *Eos, Trans. Amer. Geophys. Union*, **93**, 337–344, doi:10.1029/2012EO350001.

Melhauser, C., and F. Zhang, 2014: Diurnal radiation cycle impact on the pregenesis environment of Hurricane Karl (2010). *J. Atmos. Sci.*, **71**, 1241–1259, doi:10.1175/JAS-D-13-0116.1.

Molinari, J., P. Duran, and D. Vollaro, 2014: Low Richardson number in the tropical cyclone outflow layer. *J. Atmos. Sci.*, **71**, 3164–3179, doi:10.1175/JAS-D-14-0005.1.

Trier, S. B., and R. D. Sharman, 2009: Convection-permitting simulations of the environment supporting widespread turbulence within the upper-level outflow of a mesoscale convective system. *Mon. Wea. Rev.*, **137**, 1972–1990, doi:10.1175/2008MWR2770.1.

——, ——, R. G. Fovell, and R. G. Frehlich, 2010: Numerical simulation of radial cloud bands within the upper-level outflow of an observed mesoscale convective system. *J. Atmos. Sci.*, **67**, 2990–2999, doi:10.1175/2010JAS3531.1.

Waco, D. E., 1970: Temperatures and turbulence at tropopause levels over Hurricane Beulah (1967). *Mon. Wea. Rev.*, **98**, 749–755, doi:10.1175/1520-0493(1970)098<0749:TATATL>2.3.CO;2.

WMO, 1957: Meteorology—A three-dimensional science. *WMO Bull.*, **6**, 134–138.

——, 1998: Manual on codes. Vol. I.1 (Part A: Alphanumeric codes). WMO Publ. WMO-306, 466 pp.

Zovko-Rajak, D., and T. P. Lane, 2014: The generation of near-cloud turbulence in idealized simulations. *J. Atmos. Sci.*, **71**, 2430–2450, doi:10.1175/JAS-D-13-0346.1.